Optimization of Electrically Controlled Permanent Magnet Synchronous Machine to Improve Flux Control Range

P. Paplicki[1]
[1]*Department of Power Systems and Electrical Drives, West Pomeranian University of Technology, Szczecin, Sikorskiego 37, 70-313 Szczecin, Poland*
paplicki@zut.edu.pl

[1]***Abstract*—This paper presents the design, analysis, control, optimization and experimental evaluation of an Electrically Controlled Permanent Magnet Excited Synchronous Machine (ECPMSM) possessing field-control capability. In order to increase flux control range of the machine a three-dimensional finite element analysis (3-D FEA) and the GOT-It software optimization tool are used. The experimental results of no-load back electromotive force (back-EMF) waveform of the prototype machine and a comparison between the analysis and test results are also presented.**

***Index Terms*—Electric vehicles, finite element methods, optimization, permanent magnet machines, field-weakening.**

I. INTRODUCTION

PM brushless machines have become widely used for traction applications of electric vehicles (EVs), mainly due to their high efficiency, high power density, high drive performance and maintenance-free qualities. However, in these applications, they often suffer from uncontrollable magnetic flux, thus limiting their constant power operation in high speed regions.

The common method to achieve high efficiency of energy conversion in the lower speed range of the PM machine is over-sizing dimensions of PMs and reducing losses. It gives an increased magnetic flux density, and the required output torque of the machine is obtained by minimized stator currents. The advantage of the method is connected with challenges in the high speed operation range.

Thus, to cope with a wide speed range, optimal motor drives for hybrid or battery electric vehicle applications should offer a field weakening machine capability of 1:4 or even 1:5. There are many ways of solving this problem that have been described in literature, e.g. [1]–[16].

In general, it can be concluded that obtaining field weakening in PM machines by eliminating detrimental effects of *d*-axis current injection has been of great interest to machine designers. Moreover, thanks to advances in material technologies, such as PMs, magnetic steels and composite materials with iron powder, have allowed to arrive at new unconventional machine configurations.

Manuscript received December 13, 2013; accepted October 14, 2014
This research was funded by a grant (No. N N510 508040) from the Ministry of Education and Science, Poland.

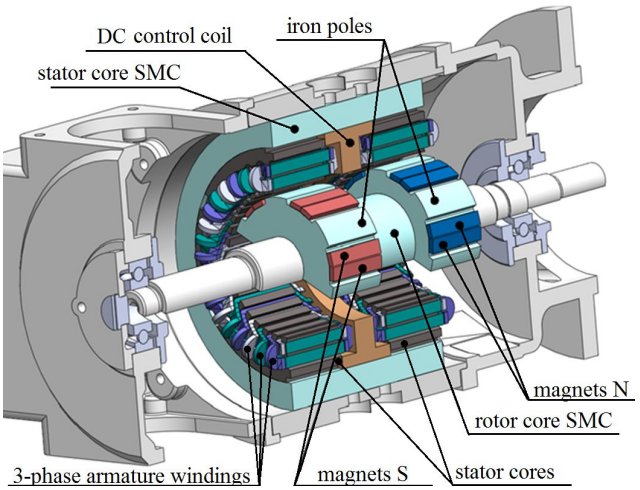

Fig. 1. Cross section of the prototype ECPMSM machine with the double surface-mounted PM rotor and 3-phase windings stator structure with a fixed DC excitation control coil.

The purpose of this paper is to present a design optimization of the ECPMSM machine in order to improve its over-speed capability using 3-D FEA.

II. MACHINE DESIGN

In order to realize field excitation control to increase or decrease the magnetization level of the machine an auxiliary direct current (DC) control coil is centrally mounted inside the stator core SMC, between two laminated stators, and it can be supplied by a 2Q-DC-chopper via stator-fixed terminals. This allows to vary the effective excitation field and the induced voltages in the armature winding.

Figure 1 shows a three-phase (3-phase) prototype ECPMSM machine with a 12-pole double inner rotor topology and two sheeted stator cores. Armature windings are located in 36 slots in each of the two stator stacks. On the one side of the machine, the rotor is formed by the exhibited single polarity PMs along with iron poles made from a soft magnetic composites (SMC) material. On the other side of the machine, the same arrangement is positioned with PMs of inverse polarity.

The flux generated by PM's passes through the laminated

stator cores pole pieces, and it crosses the air-gap of the machine in the radial direction. A main portion of the flux is passed through the stator core SMC in the axial direction, and it is returned via the rotor core SMC. The remaining part of the flux excited by PM passing through the stator cores returns to the iron pole SMC of the rotor. The flux passing through the iron pole is very important from the point of view of a field-weakening capability.

The main design data of the prototype ECPMSM machine is listed in Table I.

TABLE I. MAIN DESIGN DATA.

Maximal constant power	1.0 kW
Speed range	0-3000 rpm
Rotor outer diameter	76.5 mm
Stator outer diameter	165.0 mm
Stator stack length	2 × 40.0 mm
Air-gap length	3.0 mm
NdFeB-PM dimensions (width x thickness)	8×3 mm
NdFeB-PM remanence	1.2 T

Active stator and rotor parts of the prototype ECPMSM machine are shown in Fig. 2.

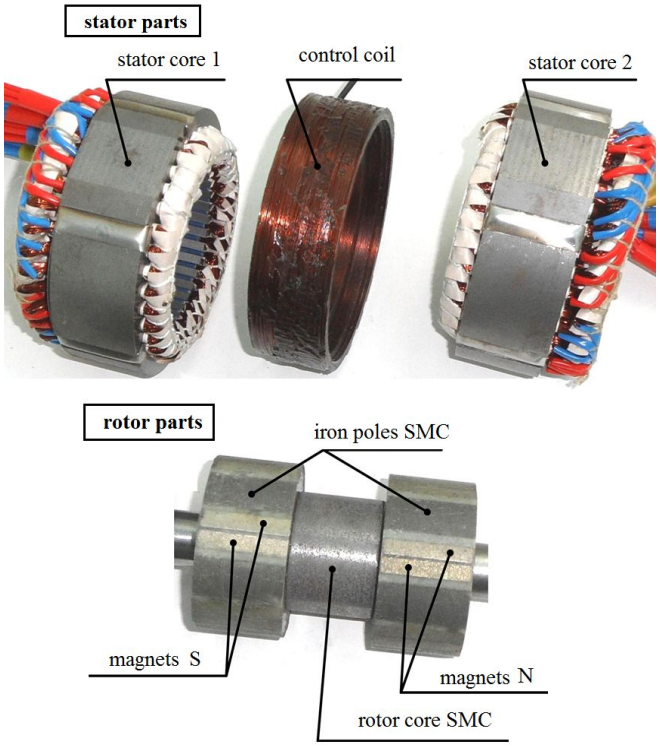

Fig. 2. The stator and rotor parts of the prototype ECPMSM machine.

In order to determine both the field weakening and strengthening capability of the prototype machine, experimental results have been employed.

The results show that the field control range of the machine is too small and insufficient from the standpoint of EVs application. Therefore, to achieve a better design solution for increasing the field weakening and strengthening capability of the machine, optimization techniques based on a genetic algorithm (GA), along with the 3-D FEA, have been applied.

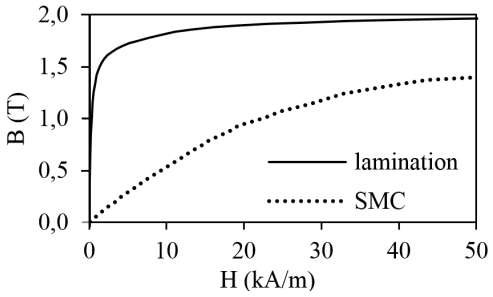

Fig. 3. Magnetization curves of the laminated material and the SMC.

To accurately calculate various components of a no-load magnetic flux density and to predict the back-EMF range, an output torque and a cogging torque of the machine, an adequate initial three-dimensional finite element model-I (3-D FEModel-I) was developed, taking into account nonlinear B-H curves and the machine's lack of the symmetry.

Figure 3 shows magnetization curves for the laminated and the SMC materials, which have been used in the prototype machine and during the 3-D FEA.

III. PERFORMANCE ANALYSIS

The optimal design of the machine is based on a precise mathematical model, which consists multiple dependent and independent parameters. There are three important, independent geometry parameters characterizing the weakening and strengthening capability of the prototype machine: thickness of magnets -d_1, length of the air-gap in front of the PM pole -$¢_m$ and length of the air-gap in front of the iron pole -$¢_{ip}$.

During optimization, the independent geometry parameters are fixed in the range: d_1 = 1.0 mm to 5.0 mm, $¢_m$ = 0.5 mm to 4.0 mm and $¢_{ip}$ = 0.5 mm to 4.0 mm.

The 3D-FEModel-I, shown in Fig. 4(a), is developed using commercial Flux3D v.10.4.2 software and used throughout optimization and 3-D FEA, and it contains approximately 280 000 nodes. Moreover, magnetic flux distribution within the 3-D FEModel-I without DC excitation control coil current has been shown in Fig. 4(b).

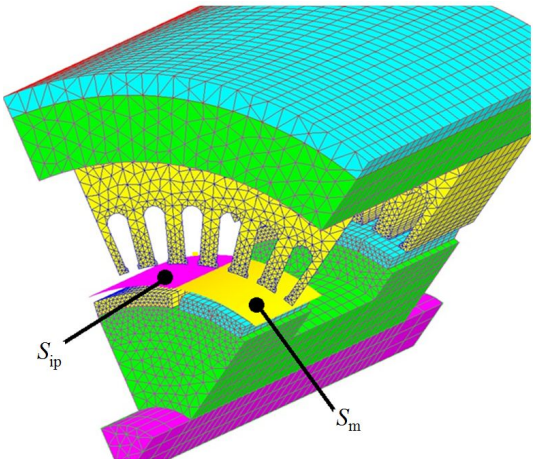

a)

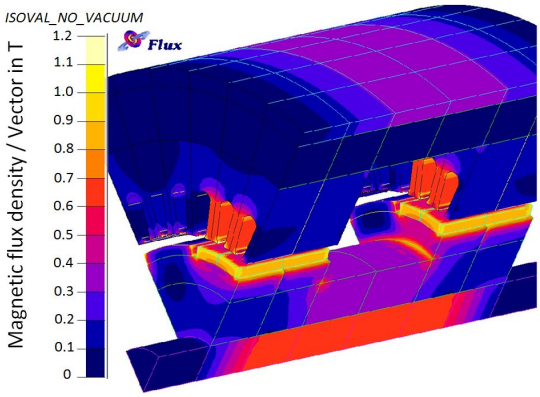

b)

Fig. 4. FEModel-I of the ECPMSM machine. (a) Meshed model with integral air-gap faces. (b) Magnetic field distributions.

In order to confirm the accuracy of the 3-D FEModel-I results, they have been compared with several experimental results. Figure 5(a) shows comparison of the no-load back-EMF waveforms at 1000 rpm rotor speed for different magnetization levels of the machine between experimental and 3-D FEA simulations. In addition, Table II lists predictions obtained from the 3-D Model-I and optimized 3-D FEModel-O within 3-D FEA both with the following values measured: the root mean square (rms) of back-EMF, aV = U_{st}/U_{weak} where U_{st}, U_{weak} are rms value of back-EMF voltages with field strengthening and weakening respectively, T_{av} – average electromagnetic torque, and the geometry parameters d_1, ¢$_m$, ¢$_{ip}$.

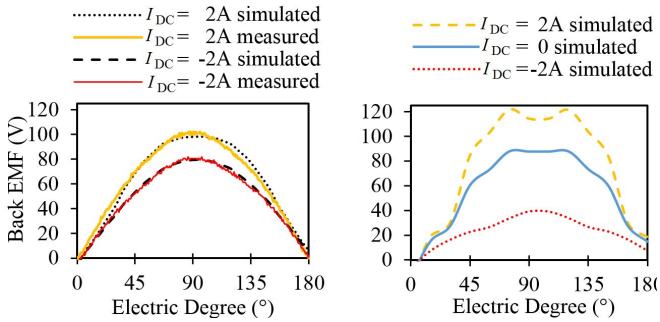

Fig. 5. Back-EMF waveforms under different magnetization level. (a) Comparison between 3-D FEModel-I and experiment. (b) Predicted by 3-D FEModel-O.

TABLE II. BACK-EMF (AT 1000 rpm), RATED TORQUE AT DIFFERENT EXCITATION CURRENT CONTROL COIL, GEOMETRY PARAMETERS AND FACTORS.

I_{DC} (A)		Simulated			Measured		
		-2.0	0	2.0	-2.0	0	2.0
3-D FEModel-I initial	Back EMF (V)	63.0	56.6	71.3	62.0	56.1	71.0
	aV	1.13			1.14		
	T_{av} (Nm)	2.7	3.3	4.1	2.9	3.3	3.8
	d_1/¢$_m$/¢$_{ip}$ (mm)	3/3/3					
	aB$_1$/aB$_2$/aB$_m$/aB$_{ip}$	0.51/0.33/0.26/0.44			-		
3-D FEModel-O optimal	Back EMF (V)	26.5	64.9	88.6	-	-	-
	aV	**3.34**			-		
	T_{av} (Nm)	1.9	3.51	5.8	-		
	d_1/¢$_m$/¢$_{ip}$ (mm)	3.915/3.78/1.2			-		
	aB$_1$/aB$_2$/aB$_m$/aB$_{ip}$	0.67/0.21/0.19/0.64			-		

IV. OPTIMIZATION PROBLEM

As mentioned above, the main purpose of this study was to find optimal independent geometry parameters for increasing magnetic flux control of the machine within achievable range. The goal is to optimize parameters: d_1, ¢$_m$ and ¢$_{ip}$ in order to maximize flux control range and rated torque. According to the problem formulation, a vector of design variables **x** has been defined: **x** = (d_1, ¢$_m$, ¢$_{ip}$).

Hence the objective functions were specified as:

$$f_1(\mathbf{x}) = Abs(\Phi_m(\mathbf{x}) - \Phi_{ip}(\mathbf{x})), \quad (1)$$

$$f_2(\mathbf{x}) = k_1\Phi_{mi}(\mathbf{x}) - \Phi_m(\mathbf{x}), \quad (2)$$

where k_1 = 0.8 is an assumed reducing magnet flux coefficient, Φ_m, Φ_{mi}, Φ_{ip}, are magnetic flux components passing through the air-gap created by PM, PM at initial 3-D FEModel-I and iron pole respectively, were calculated as:

$$\Phi_m = \iint_{S_m} \mathbf{B} \cdot d\mathbf{S}, \quad (3)$$

$$\Phi_{ip} = \iint_{S_{ip}} \mathbf{B} \cdot d\mathbf{S}. \quad (4)$$

By minimizing (1), the difference between fluxes passing through the magnet Φ_m and iron pole Φ_{ip} becomes small and thus increased flux control range is obtained. It should be pointed out that the optimization objective and constraint functions should be calculated while the magnetic field is weakened.

A constrained optimization problem was implemented based on an aggregated objectives function f_1(**x**) (to be minimized) and an inequality constraint function f_2(**x**) (to be ≤ 0). Furthermore, in order to find the global optimum for the optimization problem, a chaining optimizer has been used. It contained two optimizers: GA and a sequential quadratic programming (SQP), as well as a seed for the pseudo-random generator [18]. In the GA algorithm, a maximum number of generations (iterations) equal to 100 and a population equal to 30 have been used. In the SQP algorithm a maximum number of iterations, equal to 20, and a tolerance of 1.0e-6 have been employed.

The optimization results show that, for the purpose of increasing the field control range efficiently, the length values of air-gaps of the machine should be quite different. The geometry parameter ¢$_m$ should be larger than parameter ¢$_{ip}$ and they should retain a proper ratio.

Figure 6 shows the topology comparison of the 3-D FEModel before and after optimization process. As can be observed, the area of the iron pole for the optimized 3-D FEModel-O has increased substantially by reducing the air-gap length ¢$_{ip}$. Moreover, both the thickness of the magnets d_1 and the air-gap length ¢$_m$ in front of the magnets have increased slightly.

Figure 7 shows a 3-D magnetic field density distribution in the total air-gap and values of magnetic flux Φ_m and Φ_{ip} obtained by FEA for 3-D FEModel-I and 3-D FEModel-O at three different values of DC excitation control coil current (-2000-, 0-, and +2000-A turns). The results show that the weakening or strengthening magnetic field is observed more clearly in the air-gap in front of the iron pole for

the optimized model then the initial one. Moreover, the simulation results prove the principles of flux control and the potential to increase back-EMF and speed control range in the prototype.

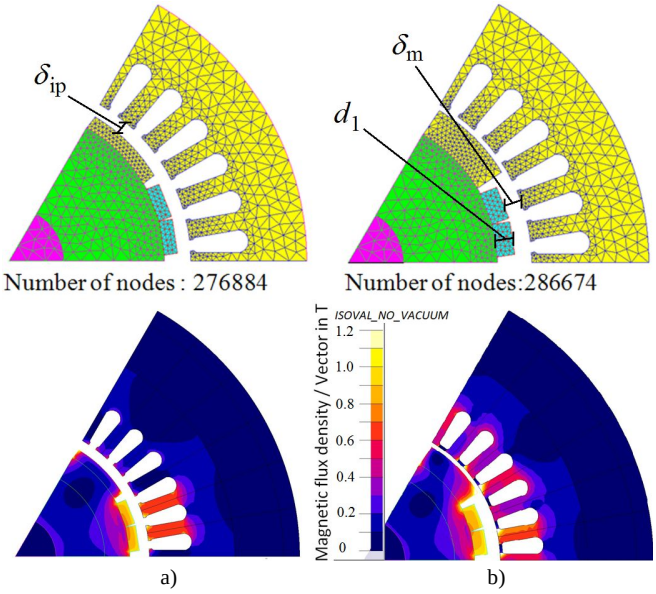

Fig. 6. Topology comparison. (a) 3-D FEModel-I. (b) 3-D FEModel-O.

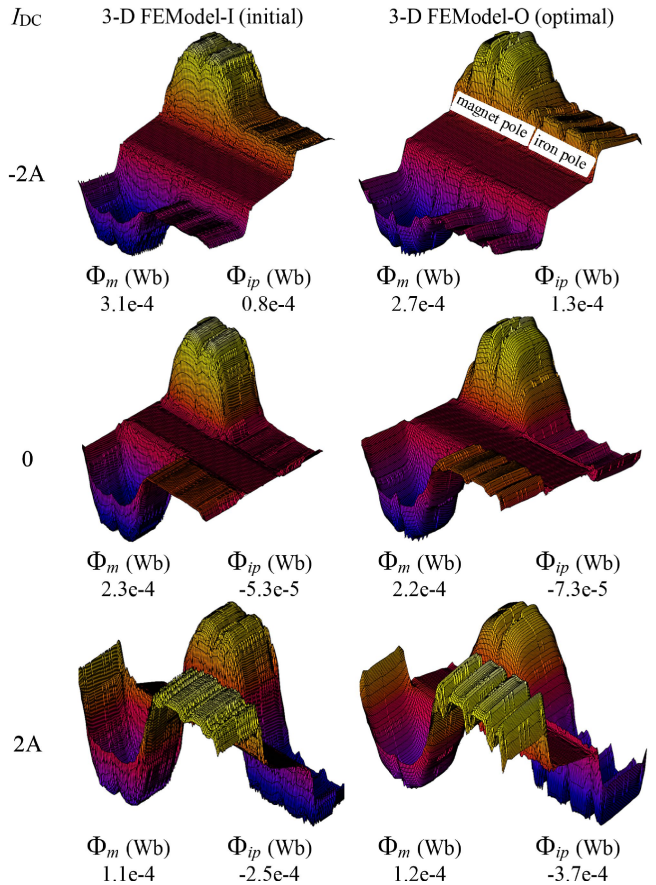

Fig. 7. 3-D air-gap normal component flux density distribution and magnetic fluxes Φ_m, Φ_{ip} of magnets and iron pole components respectively.

Figure 8 shows the air-gap magnetic flux distribution and the mean value of magnetic flux density over the magnets and iron pole sections of the rotor for extreme values of the DC excitation control coil current.

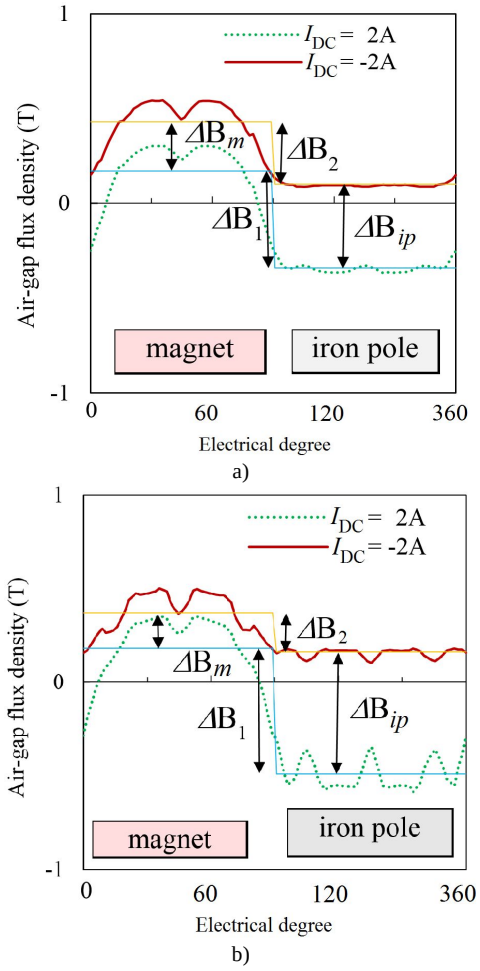

Fig. 8. Air-gap flux density. (a) 3-D FEModel-I. (b) 3-D FEModel-O.

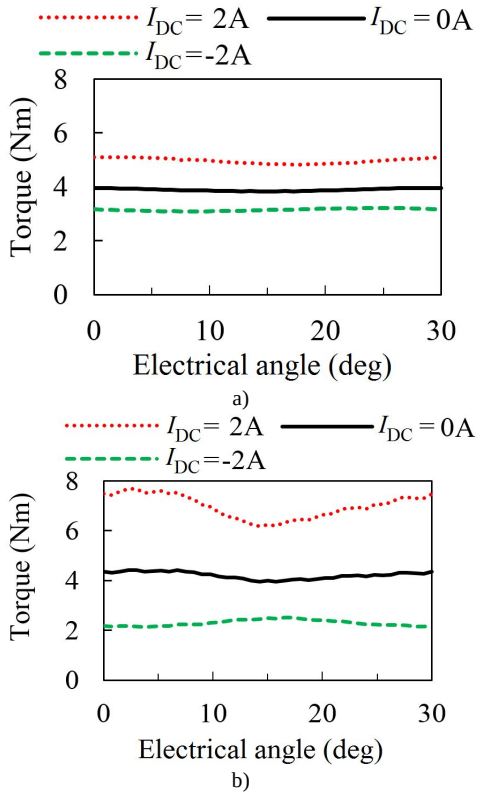

Fig. 9. Electromagnetic torque comparison by 3-D FEA. (a) 3-D FEModel-I. (b) 3-D FEModel-O.

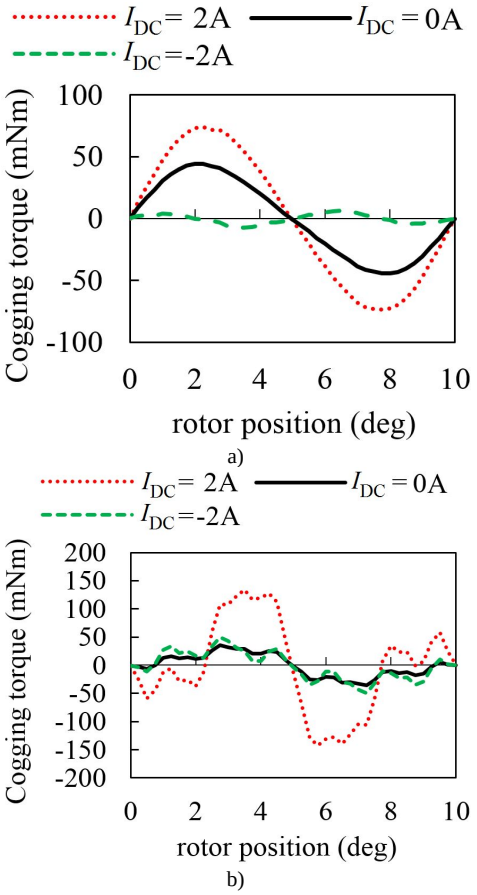

Fig. 10. Cogging torque comparison by 3-D FEA. (a) 3-D FEModel-I.(b) 3-D FEModel-O.

When compared to the initial model, the optimal 3-D FEModel-O displays an increased sensitivity to changes in magnetization level. The air-gap magnetic flux density in front of the iron pole changes its direction and magnitude in a dynamic manner (ΔB_{ip}), depending on the direction of the DC excitation control coil current. Since the PM magnetic fluxes change slightly (ΔB_m) with the excitation control coil current, the total flux in the air-gap alters with the direction of the field current and the magnitude.

The maximum range of flux control can be achieved if ΔB_2 tends towards zero. The maximum value of ΔB_1 means a significant strengthening of magnetic flux. In general, it can be assumed that the ratio of ΔB_1 to ΔB_2 determines a field-weakening ratio.

The predicted electromagnetic torque values and characteristics of the 3-D FEModel-I and 3-D FEModel-O as a function of the DC excitation control coil current are shown in Fig. 9 and Table II. As can be observed in these characteristics, electromagnetic torque in the 3-D FEModel O shows an increase of approximately 40 % at full magnetization level and a decrease of approximately 30 % in the state of weakened field compared to the 3-D FEModel-I.

Furthermore, Fig. 10 shows the cogging torque versus rotor position characteristics. The results reveal the disadvantage of rising air-gap field harmonics and increasing values of the cogging torque at full magnetization level of the optimized topology of ECPMSM machine. This may result in an increased torque ripple of the machine. Thus, in order to reduce the air-gap magnetic field harmonics for ripple torque minimization, various techniques, e.g. [18]–[24], should be used and developed.

V. CONCLUSIONS

In the paper, a new approach to optimization and the 3-D FEA-analysis of the novel ECPMSM machine have been presented. Through the use of the new optimization tool GOT-It, it was possible to set up the optimization problem easily and quickly, and to find the best configurations of the machine, according to the presented design objectives and the associated constraints. By employing the presented simulation model in the time-stepping 3-D FEA, the online magnetization characteristic and the relationships between the main design parameters and the performance requirements of the machine have been established. The back-EMF, the torque output, and the cogging torque components have also been successfully analysed.

According to 3-D FEA results contained in table II, it can be concluded that, in the optimized ECPMSM machine, a field-weakening ratio of 3.3:1 and higher can be effectively obtained. Moreover, the results show that the proposed machine can offer effective online flux control and a wide constant-power speed range, without any negative effects of current injection.

From the presented comparison between the experimental results and the results achieved from the 3-D FEA simulations of the machine, using an advanced coupling technology computation method, has revealed a satisfying level of accord.

By optimizing the shape and position of the PMs and the iron poles in the rotor, the performance of the proposed machine has been improved even further, making it more suitable for EV applications.

REFERENCES

[1] K. Ki-Chan, “A novel magnetic flux weakening method of permanent magnet synchronous motor for electric vehicles”, *IEEE Trans. Magn.*, vol. 48, no. 11, pp. 4042–4045, 2012. [Online]. Available: http://dx.doi.org/10.1109/TMAG.2012.2198444

[2] H. May, R. Palka, P. Paplicki, *et al*, “Modified concept of permanent magnet excited synchronous machines with improved high-speed features”, *Archives of Electrical Engineering*, vol. 60, no. 4, pp. 531–540, 2011. [Online]. Available: http://dx.doi.org/10.2478/v10171-011-0043-2

[3] X. Zhu, L. Quan, D. Chen, “Design and analysis of a new flux memory doubly salient motor capable of online flux control”, *IEEE Trans. Magn.*, vol. 47, no. 10, pp. 3220–3223, 2011. [Online]. Available: http://dx.doi.org/10.1109/TMAG.2011.2154358

[4] T. Kosaka, M. Sridharbabu, *et al*, “Design studies on hybrid excitation motor for main spindle drive in machine tools”, *IEEE Trans. Ind. Electron.*, vol. 57, no. 11, pp. 3807–3813, 2010. [Online]. Available: http://dx.doi.org/10.1109/TIE.2010.2040560

[5] S. Chaithongsuk, B. Nahid-Mobarakeh, J. Caron, N. Takorabet, F. Meibody-Tabar, “Optimal design of permanent magnet motors to improve field-weakening performances in variable speed drives”, *IEEE Trans. Ind. Electron.*, vol. 59, no. 6, pp. 2484–2494, 2012. [Online]. Available: http://dx.doi.org/10.1109/TIE.2011.2164770

[6] B. Nedjar, S. Hlioui, Y. Amara, L. Vido, M. Gabsi, M. Lecrivain, ”A new parallel double excitation synchronous machine”, *IEEE Trans. Magn.*, vol. 47, no. 9, pp. 2252–2260, 2011. [Online]. Available: http://dx.doi.org/10.1109/TMAG.2011.2134864

[7] M. Aydin, H. Surong, T. A. Lipo, “Design, analysis, and control of a hybrid field-controlled axial-flux permanent-magnet motor”, *IEEE Trans. Ind. Electron.*, vol. 57, no. 1, pp. 78–87, 2010. [Online]. Available: http://dx.doi.org/10.1109/TIE.2009.2028294

[8] H. May, R. Palka, P. Paplicki, S. Szkolny, M. Wardach, “Comparative research of different structures of a permanent-magnet excited synchronous machine for electric vehicles”, *Electrical*

Review, no. 88, vol. 12a, pp. 53–55, 2012.

[9] J. Wang, X. Yuan, K. Atallah, "Design optimization of a surface mounted permanent magnet motor with concentrated windings for electric vehicle applications", *IEEE Trans. on Vehicular Technology*, vol. 62, no. 3, pp. 1053–1064, 2013. [Online]. Available: http://dx.doi.org/10.1109/TVT.2012.2227867

[10] V. I. Patel, J. Wang, "Assessment of 12-slot, 14-pole permanent magnet flux switching machine with hybrid excitation for electric vehicle application", *IEEE Energy Conversion Congress and Exposition (ECCE 2013)*, pp. 5092–5099, 2013. [Online]. Available: http://dx.doi.org/10.1109/ECCE.2013.6647388

[11] K. Nguyen-Thac1, T. Orlowska-Kowalska, G. Tarchala, "Comparative analysis of the chosen field-weakening methods for the Direct Rotor Flux Oriented Control drive system", *Archives of Electrical Engineering*, vol. 61, no. 4, pp. 443–454, 2012.

[12] S. Duan, L. Zhou, J. Wang, "Flux weakening mechanism of interior permanent magnet synchronous machines with segmented permanent magnets", *IEEE Trans. Applied Super-conductivity*, vol. 24, no. 3, 2014.

[13] Jiabin Wang, Xibo Yuan, K. Atallah, "Design optimization of a surface-mounted permanent-magnet motor with concentrated windings for electric vehicle applications", *IEEE Trans. Vehicular Technology*, vol. 62, no. 3, pp. 1053–1064, 2013. [Online]. Available: http://dx.doi.org/10.1109/TVT.2012.2227867

[14] S. Hemmati, T. A. Lipo, "Field weakening of a surface mounted permanent magnet motor by winding switching", *Int. Symposium on Power Electronics, Electrical Drives, Automation and Motion (SPEEDAM)*, pp. 736–740, 2012. [Online]. Available: http://dx.doi.org/10.1109/SPEEDAM.2012.6264472

[15] A. Sarikhani, O. Mohammed, "Demagnetization control for reliable flux weakening control in PM synchronous machine", *IEEE Trans. Energy Conv.*, vol. 27, no. 4, pp. 1046–1055, 2012. [Online]. Available: http://dx.doi.org/10.1109/TEC.2012.2217968

[16] P. Paplicki, "The new generation of electrical machines applied in hybrid drive car", *Electrical Review*, vol. 86, no. 6, pp. 101–103, 2010.

[17] GOT-It Tutorial, *CEDRAT*, October 2011. [Online] Available: http://www.cedrat.com

[18] P. Di Barba, M. E. Mognaschi, R. Palka, P. Paplicki, S. Szkolny, "Design optimization of a permanent-magnet excited synchronous machine for electrical automobiles", *JAEM*, *IOS Press*, vol. 39, no 1–4, 2012, pp. 889–895, 2012.

[19] P. Di Barba, M. E, Mognaschi, R. Palka, *et al*, "Optimization of the MIT field exciter by a multiobjective design", *IEEE Trans. on Magn*., vol. 45, no. 3, pp. 1530–1533, 2009.

[20] P. Putek, P. Paplicki, M. Slodicka, R. Palka, "Minimization of cogging torque in permanent magnet machines using the topological gradient and adjoint sensitivity in multi-objective design", *JAEM*, *IOS Press*, vol. 39, no. 1–4, pp. 933–940, 2012.

[21] M. Wardach, "Cogging torque reducing in electric machine by poling modification of magnetic circuit", *Electrical Review*, no. 2, pp. 131–133, 2009.

[22] P. Putek, P. Paplicki, M. Slodicka, *et al*, "Application of topological gradient and continuum sensitivity analysis to the multi-objective design optimization of a permanent-magnet excited synchronous machine", *Electrical Review*, vol. 88, no 7a, pp. 256–260, 2012.

[23] P. Putek, P. Paplicki, R. Palka, "Low cogging torque design of Permanent-Magnet machine using modified multi-level set method with total variation regularization", IEEE Trans. Magn., vol. 50, no. 2, article no. 7016204, 2014. [Online]. Available: http://dx.doi.org/10.1109/TMAG.2013.2286297

[24] P. Putek, P. Paplicki, R. Palka, "Topology optimization of rotor poles in a permanent –magnet machine using level set method and continuum design sensitivity analysis", COMPEL, vol. 33, no. 3, pp. 711-728, 2014. [Online]. Available: http://dx.doi.org/10.1108/COMPEL-09-2013-0286